Research Article

Light-induced Trp_{in}/Met_{out} Switching During BLUF Domain Activation in ATP-bound Photoactivatable Adenylate Cyclase OaPAC

Anaïs Chretien [1,2], Marius F. Nagel [3], Sabine Botha [4,5], Raphaël de Wijn [1], Lea Brings [1], Katerina Dörner [1], Huijong Han [1], Jayanath C. P. Koliyadu [1], Romain Letrun [1], Adam Round [1], Tokushi Sato [1], Christina Schmidt [1], Radu-Costin Secareanu [1], David von Stetten [6], Mohammad Vakili [1,†], Agnieszka Wrona [1], Richard Bean [1], Adrian Mancuso [1,‡], Joachim Schulz [1], Arwen R. Pearson [7], Tilman Kottke [3], Kristina Lorenzen [1] and Robin Schubert [1,*]

*1 - **European XFEL GmbH,** Schenefeld, Germany*
*2 - **Department of Chemistry,** Universität Hamburg, Hamburg, Germany*
*3 - **Department of Chemistry and Medical School OWL,** Bielefeld University, Bielefeld, Germany*
*4 - **Department of Physics,** Arizona State University, Tempe, AZ 85287-1504, USA*
*5 - **Biodesign Center for Applied Structural Discovery,** Arizona State University, Tempe, AZ 85287-5001, USA*
*6 - **European Molecular Biology Laboratory,** Hamburg Unit, Hamburg, Germany*
*7 - **Institute for Nanostructure and Solid-State Physics,** Universität Hamburg, Hamburg, Germany*

Correspondence to Robin Schubert:
https://doi.org/10.1016/j.jmb.2024.168439
Edited by Volha Chukhutsina

Abstract

The understanding of signal transduction mechanisms in photoreceptor proteins is essential for elucidating how living organisms respond to light as environmental stimuli. In this study, we investigated the ATP binding, photoactivation and signal transduction process in the photoactivatable adenylate cyclase from *Oscillatoria acuminata* (OaPAC) upon blue light excitation. Structural models with ATP bound in the active site of native OaPAC at cryogenic as well as room temperature are presented. ATP is found in one conformation at cryogenic- and in two conformations at ambient-temperature, and is bound in an energetically unfavorable conformation for the conversion to cAMP. However, FTIR spectroscopic experiments confirm that this conformation is the native binding mode in dark state OaPAC and that transition to a productive conformation for ATP turnover only occurs after light activation. A combination of time-resolved crystallography experiments at synchrotron and X-ray Free Electron Lasers sheds light on the early events around the Flavin Adenine Dinucleotide (FAD) chromophore in the light-sensitive BLUF domain of OaPAC. Early changes involve the highly conserved amino acids Tyr6, Gln48 and Met92. Crucially, the Gln48 side chain performs a 180° rotation during activation, leading to the stabilization of the FAD chromophore. Cryotrapping experiments allowed us to investigate a late light-activated state of the reaction and revealed significant conformational changes in the BLUF domain around the FAD chromophore. In particular, a Trp_{in}/Met_{out} transition upon illumination is observed for the first time in the BLUF domain and its role in signal transmission via α-helix 3 and 4 in the linker region between sensor and effector domain is discussed.

Introduction

Light-sensitive photoreceptors evolved in all domains of life, enabling organisms to respond to light variations in their environment. Photoreceptors include a light sensor domain, examples for blue light sensitivity are Light, Oxygen, or Voltage (LOV) domains or Blue Light sensors Using FAD (BLUF) domains.[1] Both offer interesting applications in optogenetics and synthetic biology.[2–15]

BLUF photoreceptors can be found in both bacteria and in eukaryotes.[1,16] They were first discovered in the unicellular flagellate *Euglena gracilis*, in which BLUF regulates the photoactivated adenylate cyclase (PAC) activity.[17] Later, two smaller multi domain BLUF photoreceptors were found in *Beggiatoa* sp. (bPAC)[11,18,19] and in *Oscillatoria acuminata* (OaPAC),[20–22] in which they control the enzymatic activity of the linked adenylate cyclase (AC) effector domains. Sequence identity between bPAC and OaPAC is around 58% and the published crystal structure of bPAC (PDB 5M2A) by Linder et al. shares the same overall secondary structure with OaPAC.[18] All BLUF domains exhibit a similar overall structure with an alpha/beta-sandwich ferredoxin-like fold containing a five-stranded β-sheet and two antiparallel α-helices (βαββαββ topology) (Figure 1A). The flavin-based chromophore binds between the two α-helices on top of the β-sheet.[1]

Due to the small size of 350 or 366 amino acids and their low dark state activity, these two photoreceptors have generated an increased interest in understanding their mechanism in order to use them as optogenetic tools.[11,12]

PAC from the cyanobacterium *Oscillatoria acuminata* is a 366 amino acid long protein that forms a homodimer containing an N-terminal BLUF sensor domain coupled to an adenylate cyclase (AC) effector domain, the latter being involved in the conversion of ATP into cyclic-AMP (cAMP) (Figure 1A). cAMP is an important second messenger and plays a crucial role in diverse signaling pathways, such as the mediation of various responses via binding to proteins of the cAMP-receptor protein family in bacteria.[7,23,24]

The previously reported crystal structures of OaPAC (PDB 4YUS, 4YUT) disclosed the conformation of the flavin binding pocket of the BLUF domain involving a conserved tyrosine (Tyr6), glutamine (Gln48) and methionine (Met92) in its Met_{in} conformation.[20] Previous studies have shown the important role of the tyrosine and the glutamine to initiate the photocycle after excitation of oxidized FAD and the signal transmission in the BLUF domain.[1,6,21,25–37] Accordingly, flavin and tyrosine radicals have been identified as intermediates, which then yield a glutamine tautomer and oxidized FAD in the light state. The semi-conserved tryptophan (Trp90) is present for OaPAC in the Trp_{out}/Met_{in} conformation in its dark state, which is similar to other BLUF photoreceptors such as bPAC (PDB 5M2A),[18] TePixD /TII0O7849 (PDB 1X0P),[38] BlrP1 (PDB 3GFZ),[30] BlrB (PDB 2BYC)[39] and BlsA (PDB 6W6Z).[40] In OaPAC, the α-helix 3 on the opposite face of the FAD binding pocket of the BLUF domain interacts with its symmetry mate in the dimer interface to form a coiled coil.[20]

After comparing the structure of OaPAC in its dark and light state, Okhi *et al.* suggested that the Cγ—Cδ bond of glutamine (Gln48) rotates approximately 40°, changing the hydrogen bond network around the isoalloxazine ring and especially between the FAD O4 and the Nε2 atom of Gln48, which could involve a glutamine tautomerization.[21] Mutational studies also suggested that the α-helix 3 bundle is related to the signal transmission from the BLUF domain to the AC domain in order to control the active site.[20]

In the proposed mechanism of bPAC from Linder *et al.*, the conformation of the tyrosine and glutamine residues are linked to a kink in β-sheet 4.[18] They also proposed that the loop between β-sheet 9 and β-sheet 10, called the tongue region, is at a central position to act as a lever that facilitates the opening of the AC domains for both subunits. With these, the active site, located at the interface between both AC domains, opens up to enable ATP turnover.

There is an ongoing debate about the presence of a Trp_{in} conformation in some of the BLUF photoreceptor structures[32,33,41] and the importance of $Met_{in/out}$ and $Trp_{in/out}$ conformations in the signal transmission,[30,42–44] but to our knowledge none of the crystallography studies have yet shown a Trp/Met switch after photoactivation in PAC photoreceptors.[18,21]

A study on the C-terminal region of OaPAC suggested that the C-terminal region regulates the adenylate cyclase activity, hence inhibiting cAMP production.[22] Therefore, the deletion of the C-terminal region of OaPAC increases enzymatic activity and enables higher sensitivity to light.

Despite the large number of studies on the light excitation in OaPAC discussed above, the signal transmission to the AC domain and the overall regulatory mechanism remain elusive. Our study, combining time-resolved crystallography with FTIR spectroscopic analysis, provides information on the mechanism after excitation of OaPAC including the early steps of the signal transmission and allosteric communication of BLUF and AC domain. We demonstrate that photon absorption by the FAD upon photoexcitation leads to a change in the hydrogen bonding network between the conserved tyrosine, the strictly conserved glutamine and the FAD chromophore. This causes the glutamine to rotate 180° and the methionine to move into a Met_{out} conformation. The semi-conserved tryptophan is therefore able to adopt a Trp_{in} conformation, enabling a straightening of the

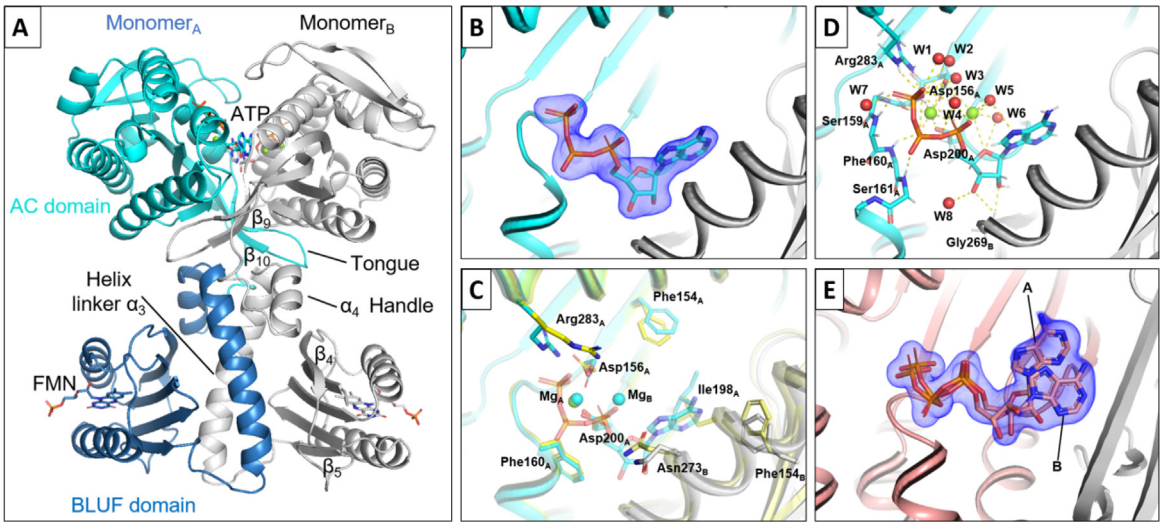

Figure 1. Dark-state structural model of holo OaPAC and details of ATP coordination in the active site. (A) Visual representation of holo OaPAC with BLUF domain (blue), AC domain (cyan) of one OaPAC monomer and the second monomer in grey. To each monomer, one FMN is bound in the BLUF domain and one ATP and two magnesium ions are bound to the AC domain. (B) ATP binding in a single conformation at cryogenic temperature is visible without bias, as shown by the F_o-F_c Polder map contoured at 3σ. (C) Side chain movements upon ATP binding at cryogenic temperature (yellow = ATP-free, cyan/grey = holo). The movements mainly involve Asp156$_A$, Ile198$_A$, Aps200$_A$, Arg283$_A$, Phe154$_B$, Asn273$_B$. Additionally, two magnesium ions are involved in the coordination of ATP, while only one magnesium ion (Mg$_A$) is present in the ATP-free state. (D) Detailed view on the ATP coordination at cryogenic temperature via hydrogen and magnesium coordination bonds by 2 magnesium ions (Mg$_A$ and Mg$_B$), water molecules, Asp156$_A$, Ile157$_A$, Ser159$_A$, Phe160$_A$, Ser161$_A$, Asp200$_A$, Arg283$_A$ and Gly269$_B$. The ribose and adenine are flipped by 180° around the adenine N1-N9 axis, revealing that ATP binds in an energetically unfavorable conformation for cAMP production in the dark. (E) ATP binding in two different conformations at room temperature is visible without bias, as shown by the F_o-F_c Polder map contoured at 3σ (red = monomer$_A$, grey = monomer$_B$). Both conformations have approximately 50% occupancy and they differ by the orientation of their ribose and the position of the adenine.

β-strand 5 and further transmitting the signal to the central coiled coil α-helix 3 and the α-helix 4 handle. Our crystallographic data also allow us to observe the presence of native ATP in the OaPAC active site, bound initially in a native but energetically unfavorable conformation for ATP turnover.

Results and Discussion

Binding coordination of ATP in the OaPAC active site

In order to unveil the details of native ATP-binding in OaPAC, crystals of OaPAC with FAD and ATP (referred to as holo-form) and with FAD but without ATP (referred to as ATP-free) were analyzed with X-ray crystallography.

OaPAC was grown in an orthorhombic crystal form in the dark. A structural model of ATP-free OaPAC could be solved at 1.5 Å resolution at cryogenic temperature and a visual representation of the model is shown in Supplementary Figure S1. OaPAC was found to bind both flavin mononucleotide (FMN) and FAD molecule in solution, but the FAD molecule bound in the BLUF domain was modeled as FMN, as the AMP moiety was not visible in the electron density. The ATP-free OaPAC structure is significantly different to the structures solved by Okhi *et al.*, where the protein crystallized either in a hexagonal space group (PDB 4YUS) with 2.2 Å Cα RMSD, or in an orthorhombic space group (PDB 4YUT) with 2.4 Å Cα RMSD, although the overall secondary structure is comparable (Supplementary Figure S1).[20] The differences are most likely due to the distinct crystal packing for each structure and hence some domains being forced to adopt a certain conformation depending on the neighboring proteins in the crystals. OaPAC co-crystallized with ATP in the dark led to a structural model with ATP bound in the active site solved at 2.1 Å (Figure 1A). As the OaPAC dimer interface forms two active site pockets, two ATP molecules are bound to the holoenzyme. An F_o-F_c Polder map contoured at 3 σ reveals binding of ATP in the active site (Figure 1B). This finding represents the first structure of native ATP bound to a wild-type photoactivatable adenylate cyclase, as so far ATP has only been observed in a mutated, constitutively active version of bPAC.[18] A comparison between both ATP-free and holo OaPAC reveals which side chains around the active site move upon ATP bind-

ing and are involved in ATP coordination (Figure 1C). Notably, only one magnesium ion Mg_A is bound in the ATP-free OaPAC structure, while two magnesium ions are involved in ATP coordination in the holo structure (Mg_A and Mg_B).

$Asp156_A$ rotates around 80° and interacts with Mg_A and W3 in order to enable ATP binding coordination in cooperation with $Asp200_A$. The latter, which is involved in the coordination of Mg_A in both structures, also rotates 30° to coordinate with the second Mg_B ion, not present in the ATP-free OaPAC structure. $Ile198_A$ is strongly displaced after 180° rotation of its side chain to enlarge the hydrophobic pocket for the adenosine in the active site. The $Phe154_B$ side chain moves closer to the adenine moiety (3.6 Å in holo vs 3.9 Å in ATP-free OaPAC). $Asn273_B$ side chain rotates 180° around Cβ and by this Cγ moves 2.1 Å away to give space to the adenosine. $Arg283_A$ turns 4.2 Å away from the surface and $Arg283_A$ NH2 forms a hydrogen bond to ATP O1γ (2.9 Å) to coordinate the γ-phosphate of ATP (Figure 1D and Supplementary Figure S2A). Between β-sheet 6 and α-helix 5, $Ser159_A$, $Phe160_A$ and $Ser161_A$ are involved in binding the phosphates directly, in addition to the coordination via $Asp156_A$, $Asp200_A$, $Ile157_A$ and the two magnesium ions. The water molecules W1,3,4,5 and 7 also interact with the phosphates, forming hydrogen bonds to stabilize them. $Gly269_B$ N forms a hydrogen bond with O2′ from the ribose (3.1 Å). Notably, the adenine is not coordinated by hydrogen bonds with any other residues, but has mainly hydrophobic interactions with surrounding amino acids (Supplementary Figure S2A). W6 and W8 help with stabilization of the ribose. A water molecule near the Mg_B, which could correspond to W6 in our model, was already described as essential for the proton transfer route during ATP turnover.[45,46] In previous studies from Lindner *et al.*, it was shown that the side chain of Phe155 in bPAC mutant ($bPAC_{Y7F}$) moves away to give space for ATP binding, while Glu157 (corresponding to Aps156 in OaPAC) rotates upon ATP binding to facilitate ATP coordination via Mg_B.[47]

Grigorenko *et al.* described the most favorable ATP configuration in the AC active site based on the lowest energy barrier to initiate ATP turnover.[45] In their structure, the O3′ from the ribose is oriented towards one of the magnesium ions and is located around 3 Å away from the phosphate Pα, which enables an in-line nucleophilic attack. This conformation facilitates the proton translocation to the neighboring aspartate residue (Asp200), which corresponds to the first step of the enzymatic reaction. However, the binding of ATP substrate in our cryogenic structure differs from the one proposed by Grigorenko *et al.,* as the distance between O3′ from the ribose ring and ATP α-phosphate is too large in the presented structure (more than 5 Å away) to permit a nucleophilic O3′ attack on Pα. In our structure, the α-phosphate is rotated away from the ribose ring and the ribosyl O3′ is not coordinated by Mg_B but is facing the opposite direction. W6, coordinated by Mg_B, is therefore not able to interact with the ATP O3′ to facilitate the proton transfer route.[45] Our ATP conformation corresponds to a higher energy state and is not suitable for a low energy proton translocation. Therefore, ATP is bound in our structure in an energetically unfavorable conformation for cAMP production and requires additional structural conformational changes before the conversion to cAMP can happen.

After revealing the conformation of ATP in the active site at cryogenic temperature, analysis of the binding at room-temperature was performed to discover potential differences. A near radiation damage-free structure of OaPAC at room temperature in its dark state was determined using serial femtosecond crystallography (SFX) at the European X-ray Free Electron Laser (EuXFEL). The obtained structure is similar to the structure at cryogenic temperature with 0.40 Å Cα RMSD over 350 residues. The resolution is slightly better at room-temperature with 1.8 Å. The unit cell parameters also change from a = 54.5 Å, b = 146.4 Å, c = 104.9 Å at cryogenic temperature to a = 54.3 Å, b = 145.8 Å, c = 105.3 Å for the SFX data. The SFX structure revealed the presence of a second ATP conformation at room temperature with 50% occupancy (annotated A and B) (Figure 1E). In the second conformation B, the phosphates are only displaced 0.3 Å in comparison to the conformation A, but the ribose adopts a different conformation with a torsion angle Pα-O5′-C5′-C4′ of −164° vs. −144°. The adenine is dragged away by approximately 5 Å, changing the torsion angle C8-N9-C1′-O4′ from 45° to 77°.

Notably, the second ATP conformation does not seem to affect the structural conformation of the surrounding amino acids in the active site significantly. When comparing the single ATP conformation of our cryogenic structure to the two ATP conformations determined at room temperature, only few noticeable changes are apparent (Supplementary Figure S2A–C). We can observe the loss of a coordination bond between $Cys201_A$ and Mg_B, and the formation of hydrogen bonds between $Asn273_B$ and ATP. $Asn273_B$ gets closer to the ATP and hydrogen bonds are formed between $Asn273_B$ Nδ2 and ATP O1α (3.0 Å for ATP conformation A and 2.7 Å for ATP conformation B). Notably, $Asp156_A$ is rotated 70° at room temperature compared to OaPAC with ATP at cryogenic temperature. This enables $Asp156_A$ to interact with both magnesium ions at room-temperature, while $Asp156_A$ was interacting with Mg_A and W3 at cryogenic temperature.

Comparing both ATP conformations at room-temperature, we observe that the hydrogen and

coordination bond network is similar, with changes mainly in the bond lengths (Supplementary Figure S2B and C). However, we do notice a few changes in interaction distances in ATP conformation B, due to the movement of the ribose closer to monomer$_B$. The distance between ATP O2′ and Gly269$_B$ is shortened from 3.8 Å to 2.4 Å, which results in formation of a hydrogen bond between them. As the adenine is mainly coordinated by hydrophobic interactions, the 5 Å displacement does not affect the surrounding residues. We do however notice additional hydrophobic interactions between the adenosine moiety of ATP conformation B and monomer$_B$ (Ile198$_B$, Met203$_B$, Ile267$_B$ and Asp270$_B$), while other hydrophobic interactions (Phe154$_B$ and Ala278$_B$), present in conformation A and in the structure at cryogenic temperature, have disappeared.

The ATP has a certain amount of room for movement in the active site, as the adenine can move freely within a 5 Å range of motion. However, both conformations found in the room-temperature structure are energetically unfavorable conformations for the production of cAMP, as described by Grigorenko *et al.*, and the binding of the most favorable ATP-conformation is not possible in the active site configuration observed in our structures.[45] As our room-temperature data also shows that the adenosine moiety is not strongly coordinated in the active site (Supplementary Figure S2B and C), it is plausible that rearrangements can occur after the AC domain opens up upon light activation.

In order to investigate if ATP can be catalytically turned over to cAMP by the studied OaPAC enzyme upon blue light excitation in solution, time-resolved light-minus-dark FTIR difference spectra were recorded for 8 minutes after excitation by an LED for 4 seconds (Figure 2A). Besides contributions from FAD and the enzyme, characteristic negative difference signals from ATP are visible in the spectral range of 900–1300 cm^{-1}.[48] Positive difference signals after blue light excitation match well with the additive signature of cAMP, pyrophosphate and phosphate in solution (Supplementary Figure S3), demonstrating that ATP is indeed turned over to cAMP by the enzyme after exposure to blue light (Figure 2B). As ATP is bound in an energetically unfavorable conformation for cAMP production in our crystals, it could be argued that this conformation is an artefact of the crystal packing. To test this hypothesis, FTIR difference spectra were recorded in the absence of ATP and showed that all main difference peaks attributed to the cyclase domain are lost when ATP is not bound, but are mostly restored in the presence of non-hydrolysable ApCpp (Supplementary Figure S4). Accordingly, it appears that the AC domain does not undergo large conformational rearrangements upon blue light excitation when ATP is not present. This leads us to the conclusion that ATP is binding to OaPAC in an energetically unfavorable conformation for cAMP production in the dark, while the cyclase domains of both monomers are closed. Our data indicate that blue light induces a conformational change along with the opening up of the AC domains only when ATP is bound, allowing the ribose and adenine moiety of ATP to rotate into a productive conformation prior to pyrophosphate cleavage and cAMP formation. Similarly, no light-dependent increase in ATP affinity was observed in bPAC$_{Y7F}$, where ATP is also bound in a non-productive conformation.[18]

To dissect the contributions to the time-resolved FTIR difference signals of OaPAC by the BLUF domain and the AC domain, a truncated mutant was analyzed that contains the BLUF domain including the long α-helix 3 linker and the α-helix 4 (OaPAC$_{1–137}$) (Supplementary Figure S5). Difference bands were accordingly assigned and labeled with squares for BLUF, triangles for AC and diamonds for ATP turnover (Figure 2A). Other signals contained mixed contributions. The difference spectra show the characteristic 1710(-) and 1695(+) cm^{-1} carbonyl signature of BLUF, which was reported for the change in hydrogen bonds to C4=O of the flavin.[49–51].

Some prominent bands originate from the AC domain as they are still present in the double difference spectrum after subtracting the OaPAC$_{1–137}$ contribution from the full-length protein (Supplementary Figure S5). Accordingly, the 1663(+) cm^{-1} band was determined to originate from the OaPAC cyclase and might correspond to the α-helical signal at around 1650 (+) cm^{-1} in bPAC.[49] It shows the same characteristic peak shape with a low frequency shoulder. Interestingly, this shoulder was attributed to the cyclase in bPAC and was lacking in the bPAC-BLUF$_{1–124}$ domain spectrum without α-helix 4 linker, whereas here a positive signal at 1655(+) cm^{-1} is observed for OaPAC$_{1–137}$ containing the α-helix 4 linker. Accordingly, we assign this signal at 1655 cm^{-1} to a response in helical structure caused by the presence of the α-helix linker 4 linking BLUF and cyclase, which has been suggested to be important for signal transfer in BLUF photoreceptors.[30,52–55]

Large difference bands from the AC domain are also present at 1626(−) and 1614(+) cm^{-1} (Supplementary Figure S5). In bPAC, the corresponding negative signal was found at 1631 (−) cm^{-1} and could be attributed by its characteristic frequency to a β-sheet response in the cyclase domain.[49] This signal is unlikely to originate from a suppressed β-sheet 5 response in the BLUF domain because signaling from FAD to α-helix 3 and α-helix-4 via β-sheet 5 is intact in OaPAC$_{1–137}$. The positive band at 1614 cm^{-1} has not been observed in bPAC[49] and YcgF[56] and is very low in frequency for an amide I signal of secondary structure elements.[57] Steady-state mea-

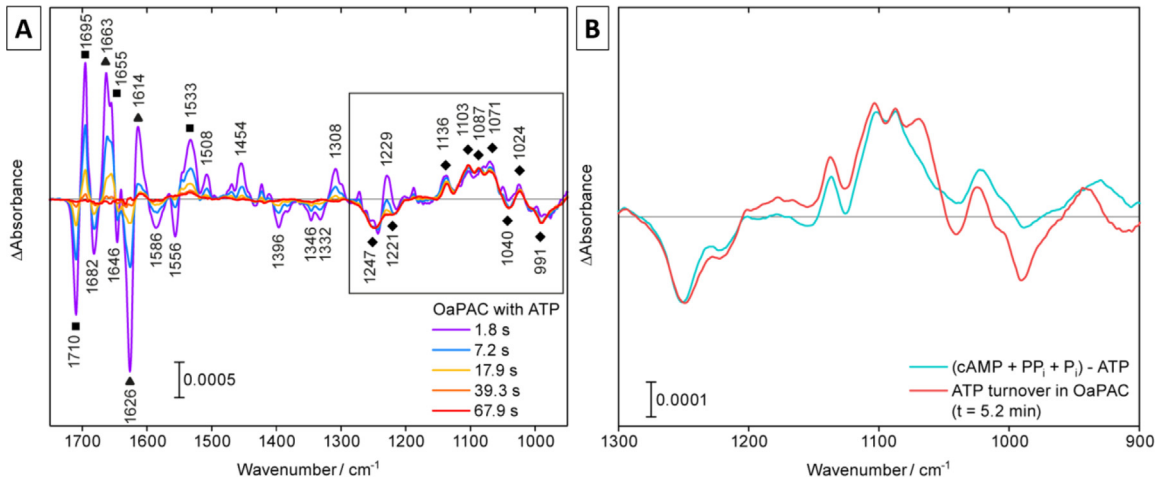

Figure 2. Light-minus-dark FTIR difference spectra of OaPAC in solution in the presence of ATP. (A) Signal evolution is observed by time-resolved FTIR spectroscopy. Assignment of contributions by the BLUF and AC domain of OaPAC to the FTIR difference signal are shown, as well as the signals attributed to ATP turnover. Specific difference bands are labelled with squares (BLUF), triangles (AC) and diamonds (ATP), other bands represent mixed contributions. The black frame indicates the spectral range that is characteristic for ATP turnover. (B) Recorded difference signal from ATP matches the expected signal of cAMP, pyrophosphate (PP_i) and phosphate (P_i) minus ATP, showing the turnover of ATP to cAMP upon blue light excitation in the FTIR difference signal.

surements on OaPAC and $OaPAC_{1–141}$ under deuterated conditions did not show any prominent positive bands in this region either,[58] which might be explained by a downshift to 1560 cm^{-1} or by band compensation effects (Supplementary Figure S5).

After assigning the contributions of both domains to the recorded difference bands, time constants for the relaxation of structural changes in the BLUF as well as the AC domain could be derived from the evolution of the FTIR difference spectra over time. For the BLUF domain in OaPAC with ATP, the signals at 1710 (–)/1696 (+) cm^{-1} decay with τ = 8 .9 ± 0.5 s. Of note, the relaxation was significantly faster in the $OaPAC_{1–137}$ mutant (τ = 6.3 ± 0.2 s) and gave similar results as full-length OaPAC in the absence of ATP (τ = 5.8 ± 0.7 s) (Figure 3). This comparison indicates that the binding of ATP and turnover to cAMP has an allosteric feedback effect on the relaxation of BLUF and its lifetime. The relaxation of the AC domain was investigated at 1615 cm^{-1} and yielded τ = 2.9 ± 0.6 s in the presence of ATP (Figure 3B), much faster than the signals of the BLUF domain. As all signals from the AC domain are lost in the FTIR spectra in the absence of ATP (Supplementary Figure 4), meaning that the AC domain is not activated without ATP bound, a relaxation without ATP could not be determined.

Signal transduction after photoexcitation in OaPAC

To better understand the reaction of BLUF photoreceptors upon photoactivation and to shed light on the differing opinions in the scientific community about the early steps of the signal transduction, a time-resolved SFX (TR-SFX) experiment was conducted at the SPB/SFX instrument at EuXFEL. Our TR-SFX study describes structural changes happening in the BLUF photoreceptor OaPAC when crystallized with ATP in the orthorhombic crystal form at two pump–probe delays (1.8 μs and 2.3 μs). The results obtained provide insight into the hydrogens bond rearrangement around the chromophore and suggest the presence of a glutamine (Gln48) rotation at 1.8 μs delay (Supplementary Figure S8A–C). The rotation of Gln48 has also been in constant discussion over the last two decades. Some spectroscopic and theoretical studies show the tautomerization of the glutamine,[27,36] accompanied by its side chain rotation,[31,37] whereas others argue that the tautomerization is not followed by any 180° side chain rotation.[21,59] While it is difficult to assign which tautomer is present with X-ray crystallography data, our TR-SFX study suggests the presence of a glutamine rotation in the early steps of photoactivation. The rotation of Gln48 was also proposed by Jung *et al.* as the PCET proton-coupled electron transfer (PCET) in AppA creates unfavorable interactions such as the proximity of the protonated FAD N5 to the amide group of Gln48 and of Tyr6 OH to Gln48 Oε1.[60] Therefore, Gln48 rotation restores favorable interactions between each of these groups. The onset of the signal transmission can be observed at 2.3 μs, where Gln48 has rotated an additional 40°, bringing the rotation to 220° compared to the dark state. Met92 moves further away

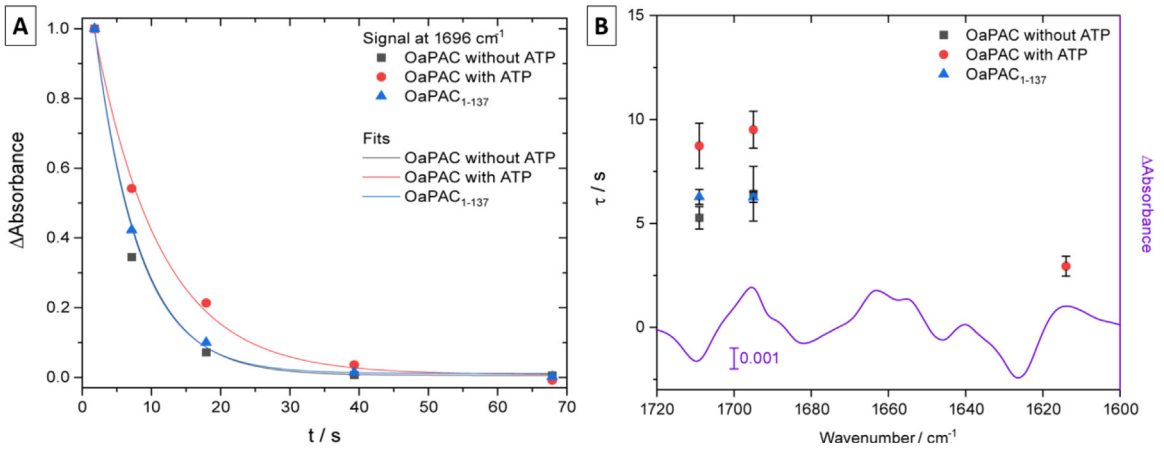

Figure 3. Kinetics of relaxation of structural changes after excitation of OaPAC derived from FTIR difference signals. (A) The evolution of the time-resolved FTIR difference absorbance was plotted at 1696 cm^{-1} for OaPAC in the presence and absence of ATP and for $OaPAC_{1–137}$ and analyzed by monoexponential functions. (B) The resulting time constants for relaxation of the BLUF domain at 1710 and 1696 cm^{-1} and for the AC domain at 1615 cm^{-1} are summarized. The AC domain shows a significantly faster relaxation (τ = 2.9 ± 0.6 s) than the BLUF domain (τ = 8.9 ± 0.5 s). Relaxation of BLUF becomes faster when ATP is absent or in the truncated $OaPAC_{1–137}$ pointing to a tight allosteric communication.

from the chromophore and induces changes in neighboring residues (Glu79 to Phe103) (Supplementary Figure S8D–F).

Some uncertainties remain in the presented TR-SFX data, such as the presence of light contamination in the subsequent dark pulse, and the difficulty to accurately calculate the absorbed photon dose by the crystals in this subsequent pulse. The results of the TR-SFX study is described in more details in the Supplementary Information (Supplementary Figure S8).

In order to investigate the later events during signal transduction from the BLUF domain to the AC domain after blue light excitation, we performed cryo-trapping experiments to capture a late stage of the reaction. A crystal of OaPAC co-crystallized with ATP was flash cooled immediately after 5 s constant light exposure. By this, full reversion to the dark state could be prevented and X-ray diffraction data of the light-activated sample were collected at 100 K at the synchrotron. The structural model of cryo-trapped OaPAC could be solved at 1.7 Å resolution.

Comparison of the structural model between the dark state and the 5 s light activated steady-state, both at cryogenic temperature, showed significant differences in the BLUF domain and especially around the flavin chromophore (Figure 4A–B), the Cα RMSD being 1.36 Å when comparing both dimers and 1.93 Å for an all-atom RMSD. Several main changes around the chromophore are important to notice. The first change involves the hydrogen bond network between the highly conserved amino acids Tyr6 and Gln48 and the flavin (Figure 4B). In dark conditions, Gln48 Nε1 forms a hydrogen bond with FMN O4 (2.9 Å) and FMN N5 (3.3 Å), and Gln48 Oε1 to Tyr6 OH (2.8 Å) (Supplementary Figure S7A). In the cryo-trapped data, the Gln48 side chain undergoes a 205° rotation and the distances of Gln48 Oε1 to FMN O4 is increased to 3.1 Å and from Gln48 Nε1 to FMN N5 to 3.4 Å, and the hydrogen bond between Gln48 Nε1 (replacing Oε1) to Tyr6 OH stretches to 3.1 Å (Figure 4B). Such change in hydrogen bond pattern to FMN O4 is in full agreement with the characteristic shifts in the IR difference spectra of BLUF domains considering that the cryo-trapped data represent a glutamine tautomer with different H-bonding properties than the glutamine of the dark state.[36] The rotation of Gln48 is similar after the continuous 5 s illumination compared to 2.3 μs delay in our TR-SFX (Supplementary Figure S8D–F). However, the displacement of the Gln48 away from Tyr6 is less pronounced (Gln48 Nε1 being 3.1 Å from Try6 OH after 5 s illumination, vs 3.5 Å after 2.3 μs). This difference is probably due to Gln48 Oε1 forming a new hydrogen bond with Trp90 Nε1 (3.4 Å). This becomes possible as Trp90 moves from the $Trp90_{out}$ conformation to a $Trp90_{in}$ conformation upon light exposure, taking the position of Met92, which is now in a $Met92_{out}$ conformation (Figure 4A and Supplementary Figure S9). The orientation of the glutamine in this model allows a favorable interaction between Gln48 Oε1 and Trp90 Nε1, which would not be the case if Gln48 had not performed a side chain rotation compared to the dark state. The formation and breakage of a hydrogen bond between the carbonyl group of Gln63 and the indole nitrogen of Trp104 in AppA was already proposed by Masuda *et al.* as critical for the light signaling pathway.[42,43] The onset of this Trp_{in} movement

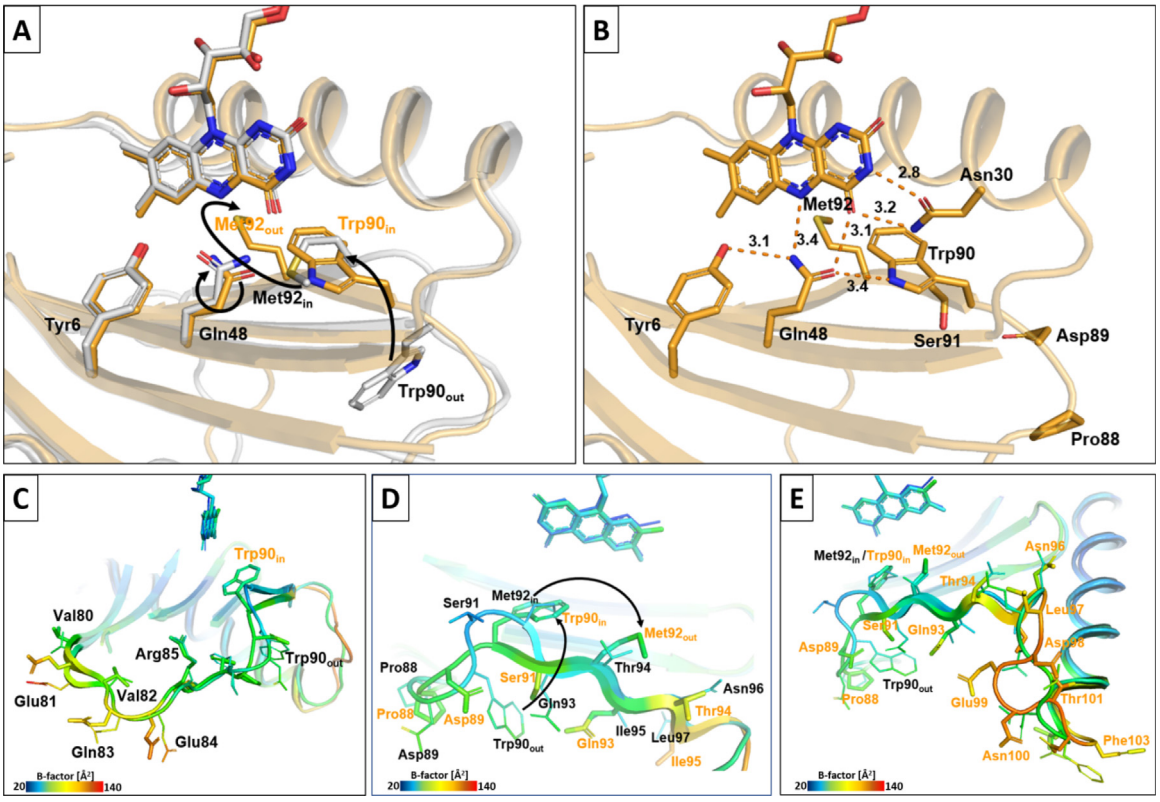

Figure 4. OaPAC shows a transition from $Trp90_{out}$ to $Trp90_{in}$ in cryo-trapped data after 5 seconds of light excitation. (A) Structural model of excited OaPAC (orange) is shown and involved amino acids in stick representation along with the dark model (grey). $Trp90_{out}$ to $Trp90_{in}$ transition as well as $Met92_{in}$ to $Met92_{out}$ transition is visualized by arrows. (B) Hydrogen bond distances around the flavin chromophore of the $Trp90_{in}$ state. (C–E) $Trp90_{in}$ transition is facilitated by mobilization of neighboring amino acids (Val80 to Leu104), as can be seen by the increase in temperature factors. Significantly displaced amino acids in the $Trp90_{in}$ model are labeled in orange. S-pattern shape of β-sheet 5 in the dark structural model straightens to accompany the two-amino acid shift in the $Trp90_{in}$ model (D). This shift is compensated by an increased flexibility in the loop between β-sheet 5 and α-helix 3 (E).

can already be seen in our TR-SFX data, where Gln48 has undergone a 180° rotation after 1.8 μs delay and Met92 flips away from the chromophore pocket at the same time, which opens up the space for Trp90 to move in (Supplementary Figure S8).

Our cryo-trapped data provide again evidence that the Gln48 rotation is an essential part of the photoactivation process. Further, it sheds light on the $Trp_{in/out}$ and $Met_{in/out}$ conformation, which has been a topic of debate since the first studies on BLUF photoreceptors. So far, it has been reported that some BLUF variants have a $Trp90_{out}$ conformation in the dark-adapted state like OaPAC,[20] bPAC,[18] AppA,[60] SyPixD/Srl1694[33] in 9 subunits out of 10, TePixD/TII0078,[38] BlrB,[39] BlrP1,[30,61] BlsA[40] while others have a $Trp90_{in}$ conformation like SyPixD/Srl1694[33] in 1 subunit out of 10 and AppA.[32,41] However, it has not been shown that the transition between both conformations occurs upon light exposure as part of the activation mechanism. Consequently, our results contradict the observations made on OaPAC before, where a 20 seconds illuminated structure only showed minor changes upon blue light excitation.[21] More precisely, the rotation of the Gln48 was reported to be only 40°, while we observe a complete rotation of the side chain. Additionally, Met92 only moved away from Gln48 after 20 seconds in the hexagonal crystal form, stretching the distance from 2.6 Å to 3.3 Å, and Trp90 only underwent a 40° rotation. Here, we observed a complete $Trp90_{in}$ conformation in combination with $Met92_{out}$ and a major structural rearrangement of the loops between β-sheet 4 and 5 and between β-sheet 5 and α-helix 3, as well as β-sheet 5 already after 5 s illumination.

It is also interesting to note that a 20 second illumination could not be performed on the orthorhombic crystal form in our study, as the resolution decreased considerably if illuminated for more than 5 seconds, and this even applied when the LED light intensity was significantly reduced. This indicates that a prolonged light exposure disrupts the crystal lattice as OaPAC undergoes its enzymatic activity. Potentially, the crystal packing for the hexagonal crystal form reported by Okhi *et al.*[21] prevented the bigger struc-

tural rearrangements needed for the Trp_{in}/Met_{out} switch. This might have also allowed the crystal to maintain high order for a longer blue light exposure, without disrupting the crystal lattice.

Brust *et al.* suggested the semi-conserved tryptophan to be a key residues in the signal transmission from the FAD chromophore to the protein backbone.[29] Studies on AppA,[44] BlrP1[30] and BlrB[59] already proposed the Trp_{out} toward Trp_{in} change in conformation to be one of the first steps in the signal transmission to the effector domain, but it has never previously been described for PAC. So far, structures of OaPAC and bPAC only showed the presence of a Trp_{out} conformation in the light-adapted state.[18,21]

The Met/Trp switch here is facilitated by a restructuring of the loop between β-sheets 4 and 5, as well as β-sheet 5 (Val80 to Asn96). The section of Pro88 to Gln93, which forms an S-pattern in the dark structure, straightens up in the 5 s cryo-trapped data and allows Trp90 to move in, causing the subsequent amino acids to move by two amino acids towards the C-terminus (Figure 4C and D). Consequently, the β-strand 5 is straightened and the temperature factors representing the atomic displacement from Gln93 to Leu104 increase to over 100 $Å^2$. In particular, the loop between β-sheet 5 and α-helix 3 (Asn96 to Leu104) becomes disordered (Figure 4E). Most likely, Aps98 to Thr101 bulges out and reduces the C-terminal shift to only one amino acid. By position Leu104 at the beginning of α-helix 3, the shift is fully compensated for and all subsequent amino acids align with the positions from the dark structure. FTIR studies by Masuda *et al.* on the AppA Trp104Ala mutant (corresponding to Trp90Ala in OaPAC) revealed that a specific signal, attributed to changes in the β-sheet structure after light activation, was eliminated by the mutation. This confirmed that the tryptophan residue is involved in the transmission of the signal through a specific β-sheet structure modification.[42] Jung *et al.* also speculated that the kink in the β-sheet 5 represents the dark-adapted state of AppA, whereas the regular β-strand corresponds to the light-adapted state.[60] Our observations agree with both proposals as they confirm the implication of Trp90 specifically in the straightening of the β-sheet 5 during the signal transmission in the light-adapted state of OaPAC.

In this study, we present strong evidence that a Met/Trp switch is present in OaPAC upon illumination that is of significant importance in the signaling mechanism. This novel observation enables us to propose Trp90 to be a main actor in the signal transduction after blue light excitation of the chromophore, dragging the entire β-strand 5 into a new conformation and inducing subsequent structural changes for signal transmission. A visual presentation of the changes around the flavin chromophore after light excitation based on the TR-SFX data and the restructuring accompanying the Met/Trp switch based on the 5 s cryo-trapped data are shown in Supplementary Video 1.

However, some questions remain, such as the specific role of the Met/Trp switch in the signal transduction. It could either be functionally relevant as an essential part of the signal transmission to the AC domain, which would take place via the α-helix 3 linking the BLUF domain to the AC effector domain; or it could be only a mechanism contributing to the stabilization of the light activated state and therefore the reason for the long-lived light-activated state of OaPAC.

The semi-conserved tryptophan residue Trp90 has been proposed to be related to the slower dynamics discovered in the signal transmission of AppA and OaPAC.[29,62] In particular, Brust *et al.* studied the relaxation pathway of AppA with vibrational spectroscopy.[29] They discovered a hierarchical pathway, where structural changes associated to H-bonded residues in the flavin binding pocket relax more slowly than changes in more distant residues. They also studied the influence of a Trp104Ala mutant in AppA (Trp90Ala for OaPAC) and revealed that the relaxation to the dark state was considerably accelerated by a factor of 80. The structural changes observed in more remote residues in AppA wild type were suppressed in the mutant, indicating that long ranged structural changes critical for the protein function did not develop without the presence of the tryptophan. These data confirm that Trp90 is a key residue in communicating the signaling state to the protein backbone in AppA and OaPAC. In addition, the importance of the α-helix 3 in signal transmission in OaPAC was proposed by Okhi *et al.*, after showing the suppression of the AC activity upon mutation of both Leu111 and Leu115, which form hydrophobic interactions between the α-helices 3 across the dimer interface.[20] They also described the loss of enzymatic activity when mutating Tyr125 (α-helix 3) or Asn256 (β-sheet 5 in the AC domain), as these two residues share an inter-subunit hydrogen bond. These two observations confirm the implication of α-helix 3 in signal transmission, with the necessity of critical non-polar and polar interactions across the dimer interface. These previous studies would support the proposal that Trp90′s function is not only to stabilize OaPAC and enable its long-lived state, but also its involvement in the mechanism contributing to the signal transmission.

Interestingly, for bPAC Linder *et al.* proposed the kink of β-sheet 4 as a pathway for signal transmission from the FAD chromophore to the α-helix 3–4 linker region before going through the tongue region of the AC domain.[18] Our data, however, do not confirm this possibility for OaPAC and tend rather toward a signal transmission via the β-sheet 5 to the α-helix 3 linker. Residues in the β-sheet 4 close to the α-helix 3 or α-helix 4 do

not show significant change upon light activation, whereas residues in the loop between β-sheet 5 and α-helix 3 exhibit strong movements with a significant increase in temperature factors in that region, confirming the involvement of the loop in the signal transmission (Figure 4C–E).

Notably, the observed changes in the cryo-trapped data versus the dark models are limited to conformational changes in the BLUF domain, while only minor changes are observed in the AC domain. Evaluation of the temperature factors on the entire structural model of OaPAC showed that they are consistently higher in the BLUF domain (Supplementary Figure S10). They confirm distinct conformational changes in the entire backbone of β-sheet 4, β-sheet 5 and α-helix 3, including the loops between them. Interestingly, the temperature factors also indicate that the α-helix 4 region is affected during signal transmission. However, the AC domain seems to be particularly stable after 5 s constant illumination and ATP is still clearly visible in the electron density. Since after a long exposure of 5 seconds before cryo-trapping the reaction is expected to progress

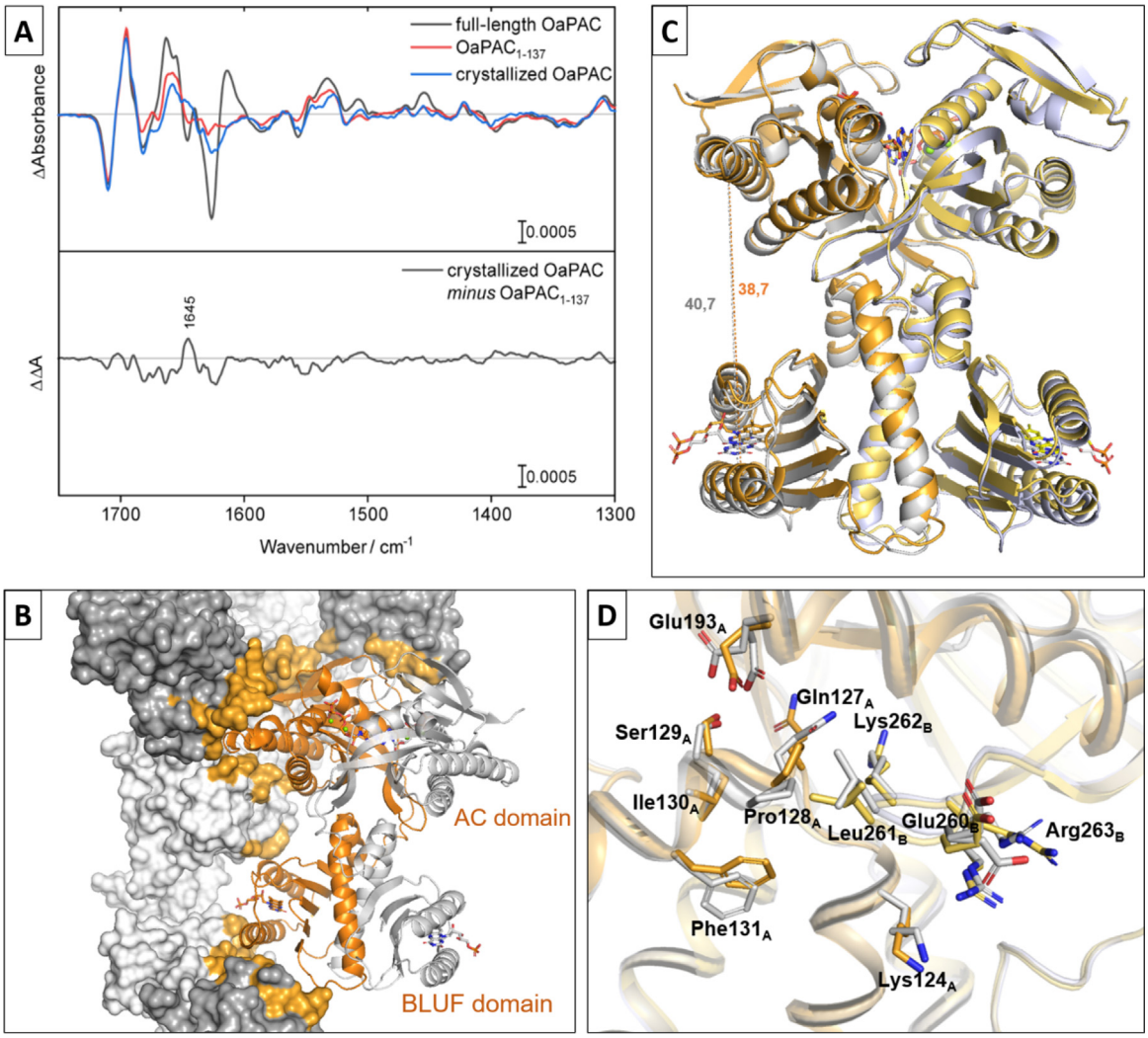

Figure 5. Analysis of adenylate cyclase (AC) domain reaction upon light exposure in orthorhombic OaPAC crystals. (A) Comparison of FTIR difference signal after blue-light exposure of OaPAC and $OaPAC_{1–137}$ in solution with OaPAC in orthorhombic crystal packing. Recorded difference signal of crystallized OaPAC matches the $OaPAC_{1–137}$ containing the BLUF domain and α-helix 3 and 4 only, showing that the AC domain is not undergoing large conformational changes in the crystal form. (B) Structural model of 5 s cryo-trapped OaPAC (orange) along with neighboring molecules in orthorhombic crystal packing as surface presentation (grey). Crystal contacts in a radius of 4 Å around OaPAC are highlighted in orange surface coloring. While the AC domain is sterically locked in place by the crystal contacts, the BLUF domain is less densely surrounded in the orthorhombic crystal packing, giving it a higher mobility. (C) BLUF domain moves about 2 Å closer to the AC domain in 5 s cryo-trapped OaPAC (orange) compared to the dark-state model (grey). (D) Side chain rearrangements in the α-helical linker region between BLUF and AC domain in 5 s cryo-trapped OaPAC (orange) compared to the dark-state model (grey).

further towards ATP to cAMP turnover, FTIR light-minus-dark difference spectra were recorded from a crystal slurry in orthorhombic space group. When comparing the spectra with those of full length OaPAC and $OaPAC_{1-137}$ in solution, it can be noted that the difference signal in the crystal packing resembles the $OaPAC_{1-137}$ containing only the BLUF domain and the α-helix 3 and 4 linker region, showing that the AC domain does not undergo large conformational changes in the crystal form (Figure 5A).

The lack in response from the AC domain upon photoexcitation in both our crystallography and FTIR data can be explained by the high number of crystal contacts present around the AC domain in the orthorhombic crystal form (Figure 5B). The analysis of the crystal packing reveals that movements of the effector domain are sterically hindered by the molecules surrounding the AC domain in the crystal. Indeed, whereas only a few crystal contacts are present around the BLUF domain, four adjacent molecules keep the AC domain locked in place with only a small margin for movement. Consequently, although the BLUF domain of OaPAC in this crystal form can be excited and conformational changes are observed as part of the activation and signal transmission up until the α-helix 4, movements in the AC domain are hindered by the tight crystal packing.

After understanding the sterically hindered reaction of the AC domain in our orthorhombic crystal form, we were able to consolidate the bigger picture of the observed changes in our cryo-trapped structure. Overall, the BLUF domain moves slightly away from the other BLUF protomer and closer to the AC domain. For example, the distance between Ile22 Cα in α-helix 1 (BLUF domain) and Glu224 Cα in α-helix 7 (AC domain) is reduced from 40.7 Å to 38.7 Å in the cryo-trapped data (Figure 5C). This movement could be with a prelude to the hinge motion of the tongue section between BLUF and AC (loop between β-sheet 9 and 10) proposed by Lindner *et al.* As the opening up of the AC domain is sterically hindered by the tight crystal packing around the AC domain (Figure 5B), only the BLUF domain is mobile upon activation. Interestingly, this movement causes a shortening of the unit cell axis a (by 2 Å) and the strong shortening of the b axis (by 5 Å) after light activation compared to the dark state at cryogenic temperature, with a = 52.5 Å, b = 141.4 Å, c = 104.7 Å and a = 54.5 Å, b = 146.4 Å, c = 104.9 Å, respectively.

The final changes observed during signal transmission can be seen in the α-helix linker (α-helix 4). Gln127 to Ser129, as well as the side chain of Phe131 shifting 1 Å closer to the tongue of the AC domain from $monomer_B$ (Figure 5D). Linder et al. proposed the tongue between β-sheet 9 and β-sheet 10 to be the link which enables signal transmission from the linker region to the AC domain for bPAC.[18] They observed a structural flexibility in that region, with the tongue being in an *up* position in one monomer and in a *down* position in the other one and suggested this flexibility is of functional relevance for the signal transmission in response to light. Notably in our structure, most of the amino acids in that region also exhibit a high flexibility, as observed by residues in α-helix 4 and the tongue region adopting multiple conformations (Figure 5D).

The changes in our structure do not contradict the idea that the signal is transmitted from the α-helix 3 to the α-helix 4, with a potential transmission to the AC domain via the tongue region. However, as the AC domain is locked in place by several crystal contacts as described above, subsequent changes in the tongue region are not observable with our crystal form.

Finally, some light induced changes are visible in the AC domain of our structure. In particular the C-terminus of OaPAC is significantly disordered in the 5 s cryo-trapped data. Glu326 and Asn327 at the end of β-sheet 13 are the last residues that can be clearly modeled in the electron density of all our modeled structures. Interestingly, their position varies substantially from the dark cryo data, confirming that the C-terminus undergoes a conformational change. As a result, the α-helix 5 seems to be destabilized as well and Asp156 to Pro168 shift slightly. This also explains why the C-terminus of OaPAC has such a strong influence on the cyclase activity,[22] as α-helix 5 is strongly involved in the coordination of the ATP phosphates.

Conclusion

Our study provides detailed insights into the binding mode of ATP in the active site of native OaPAC and its allosteric influence on the BLUF domain. ATP is mainly coordinated via the phosphate groups and is highly flexible around the adenosine moiety. While at cryogenic temperatures only one conformation is observed, two conformations can be seen at room-temperature. Although, both are an energetically unfavorable conformation for cAMP production, it could be shown that this conformation is indeed the native binding mode in OaPAC in the dark. Rotation of the ribose to a productive conformation for cAMP turnover only occurs after light activation and subsequent opening of the active site between both AC domains.

Furthermore, structural information about the early conformational rearrangements in the μs time-scale during activation of the flavin chromophore in the BLUF domain was obtained. Although some of the reported changes in bond distances are at the resolution limit of the crystallographic data, the overall changes in the hydrogen bond network between the dark state and the different light induced states are consistent. The data provide additional information

to the ongoing debate about the molecular details during flavin activation in BLUF domains. The cryo-trapped structural data reveal significant conformational changes in the BLUF domain at late reaction times. Our data provide evidence for a Trp_{in}/Met_{out} transition upon illumination, not seen in BLUF domains before. We postulate that this switch is involved in signal transmission via β-sheet 5 and the following loop to the linker region (α-helix 3 and 4) and thereby activates the AC domain. However, subsequent movements in the AC domain are hindered by the tight crystal packing. Despite these limitations, our findings contribute to the understanding of how photoreceptor proteins sense and respond to environmental light triggers, with potential implications for the development of optogenetic tools and light-responsive biotechnological applications. Further investigations into the functional implications of these conformational changes will deepen our comprehension of the intricate signaling mechanisms underlying photoactivatable adenylate cyclases.

Materials and Methods

Expression and purification of recombinant OaPAC

Sample preparation and injection testing proceeded in the immediate vicinity of the XFEL beamlines in the XBI (XFEL Biology Infrastructure) laboratories.[63]

OaPAC protein used in all experiments corresponds to residues 1 to 350 of the full length OaPAC (UniProt ID K9TLZ5) with C-terminal truncation of 16 amino acids (Supplementary Figure S11). $OaPAC_{1–137}$ protein used in the FTIR experiments corresponds to residues 1–137 of the full length OaPAC (UniProt ID K9TLZ5) with C-terminal truncation of 229 amino acids from the AC domain.

The coding sequence for OaPAC was cloned into a pColdI expression vector (TakaraBio), resulting in pColdI-OaPAC expression vector, encoding for $OaPAC_{1–350}$ in its native form without tag (Supplementary Tables 4 and 5). The coding sequence for $OaPAC_{1–137}$ was cloned into a pColdI expression vector (TakaraBio), the resulting expression vector encoded for $OaPAC_{1–137}$ carrying an N-terminal histidine tag.

pColdI-OaPAC and pColdI-$OaPAC_{1–137}$ expression vectors were transformed into *Escherichia coli* BL21*(DE3) cells, cultured in LB medium and double induced with a cold shock on ice for 5 minutes followed by 10 minutes at 12 °C, and the addition of 1 mM Isopropyl β-D-1-thiogalactopyranoside (IPTG) at an OD_{600nm} between 0.4 and 0.6. Cells were grown for an additional 16 h at 30 °C. The cells were harvested by centrifugation at 8,000*g* for 30 minutes and the cell pellet was frozen at −20 °C until use.

For OaPAC, one cell pellet was resuspended in lysis buffer containing 20 mM Tris/HCl pH 7.5, 20 mM NaCl and protease inhibitors (Roche – cOmplete™ ULTRA Tablets, Mini, EDTA-free, EASYpack Protease Inhibitor Cocktail). After resuspension, cells were lysed by 3 cycles of high-pressure homogenization and centrifuged for 1 h at 30,000*g*. The supernatant was collected and the recombinant protein was purified by fast protein liquid chromatography (FPLC). The first step involved an anion exchange chromatography with elution through a linear salt gradient to 1 M NaCl on a HiTrap Q HP 16/100 column (Cytiva). An ammonium sulfate precipitation was performed with 1.4 M ammonium sulfate. After precipitation, the solution was filtered and the buffer exchanged to 50 mM Tris/HCl pH 8.5, 50 mM NaCl using a PD10 desalting column (Cytiva). The last step consisted of a size exclusion chromatography using a gel filtration column HiLoad 26/600 Superdex 200 pg (Cytiva). Purified protein in 50 mM Tris/HCl pH 8.5, 50 mM NaCl was concentrated to 12 mg/mL, determined by A_{280} measurements using a calculated extinction coefficient of 48,910 M^{-1} cm^{-1}, flash-cooled in liquid nitrogen and stored at −80 °C until use.

For $OaPAC_{1–137}$, one cell pellet was resuspended in lysis buffer containing 10 mM HEPES pH 7.5, 20 mM imidazole, 150 mM NaCl and protease inhibitors (Roche – cOmplete™ ULTRA Tablets, Mini, EDTA-free, EASYpack Protease Inhibitor Cocktail). After resuspension, cells were lysed by 3 cycles of high-pressure homogenization and centrifuged for 1 h at 30,000*g*. The supernatant was collected and the recombinant protein was purified by FPLC. The purification of $OaPAC_{1–137}$ involved an affinity chromatography step on a HisTrap HP column (Cytiva) with elution through a linear imidazole gradient to 500 mM imidazole. After the elution, the protein solution was concentrated and injected onto a gel filtration column HiLoad 26/600 Superdex 200 pg (Cytiva) for size exclusion chromatography. Purified protein in 10 mM HEPES pH 7.5, 150 mM NaCl was concentrated to 12 mg/mL, determined by A_{280} measurements using a calculated extinction coefficient of 28,670 M^{-1} cm^{-1}, flash-cooled in liquid nitrogen and stored at −80 °C until use.

Protein crystallization and structure determination

Crystals were obtained by vapor diffusion using the sitting drop method. Crystals were grown at 4 °C for one week in the dark after mixing 500 nL OaPAC protein at 10 mg/mL and 500 nL crystallization buffer from the 50 μL reservoir containing 100 mM SPG buffer (succinic acid, sodium dihydrogen phosphate, and glycine in the molar ratios 2:7:7) pH 7.0, 1.2 M disodium succinate, 100 mM guanidine HCl and 5 mM $MgCl_2$. Before cryo cooling, a single crystal was

soaked with the reservoir solution containing 20% (v/v) glycerol under red light illumination.

200 × 60 × 40 μm^3 crystals for dark-state OaPAC grew in an orthorhombic crystal form with space group $C222_1$, with one molecule in the asymmetric unit and unit-cell parameters a = 52.9 Å, b = 146.2 Å, c = 103.6 Å, α = 90°, β = 90°, γ = 90°. The high-resolution cutoff was 1.5 Å for this data set. Diffraction data were collected at 100 K at the ID23-2 beamline at ESRF, Grenoble, France using a DECTRIS PILATUS3 X 2 M detector.[64] 3,600 frames with 20 ms exposure were recorded with a 360° rotation range and 0.1° oscillation per frame. The X-ray beam was focused to 5 × 26 μm, the energy was set at 14.2 keV and the transmission at 10%. Data recorded for the experiment at ESRF are available at data.esrf.fr/-doi/https://doi.org/10.15151/ESRF-DC-1329827085.

50 × 35 × 8 μm^3 crystals for dark-state OaPAC co-crystallized with 5 mM ATP grew in space group $C222_1$ with one molecule in the asymmetric unit and unit-cell parameters a = 54.5 Å, b = 146.4 Å, c = 104.9 Å, α = 90°, β = 90°, γ = 90°. The high-resolution cutoff was 2.1 Å for this data set. Diffraction data were collected at 100 K at the ID23-2 beamline at ESRF, Grenoble, France using a DECTRIS PILATUS3 X 2M detector.[64] 3,000 frames with 20 ms exposure were recorded with a 300° rotation range and 0.1° oscillation per frame. The X-ray beam was focused to 5 × 5 μm, the energy was set at 14.2 keV and the transmission at 1%. Data recorded for the experiment at ESRF are available at data.esrf.fr/doi/https://doi.org/10.15151/ESRF-DC-1329817123.

For the cryo-trapping experiment, a single 150 × 50 × 30 μm^3 crystal was illuminated for 5 seconds at 30 mW (10 absorbed photons per molecule) using the illumination system pE-400 (CoolLED) setup at 435 nm. The crystal was flash cooled in liquid nitrogen immediately after illumination. Light-activated OaPAC co-crystallized with 5 mM ATP grew in space group $C222_1$ with one molecule in the asymmetric unit and unit-cell parameters a = 52.5 Å, b = 141.4 Å, c = 104.7 Å, α = 90°, β = 90°, γ = 90°. The high-resolution cutoff was 1.7 Å for this data set. Diffraction data were collected at 100 K at the P11 beamline at PETRA III, Hamburg, Germany using a DECTRIS EIGER2 X 16M detector.[65] 3,600 frames with 15 ms exposure were recorded with a 360° rotation range and 0.1° per frame. The X-ray beam was focused to 50 × 50 μm, the energy was set at 12.0 keV and the transmission at 35%.

All data were processed and scaled using the program package XDS.[66] All datasets were merged using AIMLESS[67] from the CCP4 suite.[68] Initial models were obtained by molecular replacement using the PHENIX program suite[69] with the OaPAC structure from Ohki et al. (PDB 4YUS)[20] as a search model. The models were refined using both the PHENIX program suite[69] and the CCP4 suite[68] and manual building was done using COOT.[70] Synchrotron data-structure refinement statistics are shown in Supplementary Table 1 and structural models have been deposited in the Protein Data Bank under accession codes 8QFE, 8QFF and 8QFG.

All the figures representing the structural models of OaPAC at cryogenic temperature were prepared with the PyMOL Molecular Graphics System, Version 2.0 Schrödinger, LLC.[71]

Microcrystals growth and TR-SFX experiment

7 × 3 × 2 μm^3 microcrystals were grown in batch after mixing 45% (v/v) OaPAC protein solution at 12 mg/mL, 10% (v/v) seeds, produced by crushing macrocrystals with seed beads, and 45% (v/v) crystallization buffer containing 100 mM SPG buffer pH 7.0, 1.4 M disodium succinate, 100 mM guanidine HCl and 5 mM $MgCl_2$. Crystals were co-crystallized with 5 mM ATP and grown in the dark at 4 °C.

The microcrystal slurry was concentrated to 20% pellet volume (v/v) after sedimentation. The slurry was injected with a gas dynamic virtual nozzle (GDVN)[72] for a serial femtosecond crystallography (SFX) experiment at the SPB/SFX instrument of the European XFEL, Schenefeld, Germany in May 2022 (proposal 2829).[73] Data recorded for the experiment at the European XFEL are available at https://doi.org/10.22003/XFEL.EU-DATA-002829-00.

OaPAC microcrystals were photoexcited with the second harmonic of the EuXFEL pump–probe laser system at 421 nm.[74–76] The optical pump pulses were stretched from their original duration of 50 fs to 250 fs by transmission through fused silica. The optical pump had a fluence of 19.8 or 100 mJ/cm^2 per pulse with a repetition rate of 188 kHz. Under these excitation conditions, 0.6 or 3 photons were absorbed on average per molecule, respectively. The calculation of the absorbed photon number was performed according to the photon calculation Excel sheet by Grünbein et al.[77]

The X-ray probe beam was focused to 3 μm × 4 μm, with 9.3 keV photon energy, an estimated pulse length of ≤30 fs and 564 kHz intra-train pulse repetition rate. Data were acquired with the AGIPD detector operating in fixed medium gain mode.[78] TR-SFX data were collected at 5 ns and 500 ns delays in a LIGHT-DARK1-DARK2 succession pattern (every 3rd pulse within a x-ray pulse train was pumped).

TR-SFX data processing and dark structure determination

During the experiment, online monitoring was performed with Karabo[79] and OnDA.[80] Raw data were calibrated using the European XFEL's internal detector calibration pipeline. Initial hit finding was

performed using crystfel 0.10.1[81] with the following parameters (through the "Extra-xwiz" interface[82]): –peaks = peakfinder8[83] –min-snr = 6 –threshold = 2 00 –min-pix-count = 1 –max-pix-count = 2 –index ing = none –local-bg-radius = 5 –max-res = 1200 –min-peaks = 0. After manual inspection of the hit/-peak finding results, custom python scripts were then used to extract image lists with at least 7 peaks for further processing.

In a second pass, the pre-selected images were subjected to a 2nd round of hit/peak finding with the same parameters as before, apart from –max-pix-count = 20, the addition of –int-radius = 2,4,6 –min-peaks = 10 and no maximum resolution set for peak finding; Indexing was attempted using mosflm,[84] xgandalf,[85] xds[66] and dirax[86] in that order.

Images were sorted into "LIGHT", "DARK1" and "DARK2" based on the pulse IDs; the list of images were annotated accordingly and passed into the partialator program[87] from CrystFEL for merging using the "—custom-split" option, the unity model, a single iteration and max-ADU set to 110000. All datasets were merged into point group mmm, and the space group was determined to be $C222_1$ using AIMLESS[67] from the CCP4 suite.[68] The high-resolution cutoff was 1.8 Å for all data sets. The space group was $C222_1$ and unit-cell parameters a = 54.3 Å, b = 145.8 Å, c = 105.3 Å, $\alpha = 90°$, $\beta = 90°$, $\gamma = 90°$.

The overall crystal hit rate averaged 4.7% from which an average of 85.5% of images could be indexed. However, due to multiple lattices being indexed in some images, the total number of indexed patterns exceeded the total number of hits. A minimum of 40 k indexed diffraction patterns were recorded for each data set, and a detailed breakdown of hits and indexed patterns for every dataset are shown in Supplementary Table 2.

The dark structure reported in this manuscript was calculated from all of the DARK2 datasets for the 100 mJ/cm^2 laser fluence merged together for all time delays. We confirmed that no light contamination was visible in the DARK2 data sets by comparing them to a dark data set collected without optical pump laser. Data collection statistics are shown in Supplementary Table 3. The initial dark model was obtained by molecular replacement using the PHENIX program suite with the dark-state OaPAC co-crystallized with ATP solved at 100 K as search model.[69]

q-weighted Fourier difference electron density maps were calculated with Xtrapol8 using a fraction of 60,000 diffraction patterns randomly chosen from all DARK2 data collected throughout the beamtime.[88] The dark structure solved from that data set was used to phase the maps. No changes were visible when comparing LIGHT and DARK2 data sets with both laser intensities, showing that the selected time delays (5 ns and 500 ns) are too short to see changes in the electron density. However, the LIGHT-DARK1-DARK2 succession pattern was chosen as light contamination might occur in the first dark pulse data (DARK1), which could be tested for by comparing the DARK1 and DARK2 data. By investigating potentially light contaminated DARK1 data from the 100 mJ/cm^2 laser fluence exposure, strong differences surrounding the flavin chromophore became visible. This indeed indicates a light contamination of our DARK1 data. Considering the DARK1 data as an additional "light"-state results in an additional time delay of 1.773 μs (X-ray pulse period) between pump and probe pulse. Consequently, this results in a calculated delay of 1778 ns (5 ns plus 1.773 μs) and 2273 ns (500 ns plus 1.773 μs) for the DARK1 data and these new time-delays are referred to as 1.8 μs and 2.3 μs, respectively. A visual representation of the collected pump–probe pattern is shown in supplementary Figure S6. It should be noted that the aforementioned absorbed photon number calculation from the pump fluence represents the upper theoretical limit from the LIGHT data and the actual absorbed photons per molecule will be substantially lower in the light-contaminated DARK1 data. Based on this, exact photon dose could not be determined for DARK1 data, but multi-photon effects can be excluded.

After the Fourier difference electron density map calculations between the DARK1 data sets and the DARK2 data set, the occupancy of the light-activated state was determined using Xtrapol8. An occupancy of around 25% was obtained for the two time-delays. Xtrapol8 was also used to calculate extrapolated structure factor amplitudes. These extrapolated measurements generated some negative structure factor amplitudes, but only for less than 5% of structure factors, for each of the two extrapolated data sets (after 1.8 μs and 2.3 μs calculated time delays). The "fref" option was used in Xtrapol8 in order to estimate their positive values.[88] With this approach, the assumption is that a strong negative difference amplitude is a consequence of measurement errors, and consequently the negative structure factors amplitudes are replaced by their corresponding values in the observed reference data set. This approach will however slightly bias the results towards the reference state, and should therefore only be used when less than 5% of the total structure factor amplitudes are negative. The extrapolated electron density maps obtained after extrapolated structure factors determination were used to model the structural changes happening at the two time points collected.

All TR-SFX models were refined using both the PHENIX program suite[69] and the CCP4 suite[68] and manual building was done using COOT.[70] SFX data- and structure refinement statistics are shown in Supplementary Table 3 and structural models have been deposited in the Protein Data Bank under accession codes 8QFH, 8QFI and 8QFJ. All the figures representing the TR-SFX

structural models of OaPAC were prepared with the PyMOL Molecular Graphics System, Version 2.0 Schrödinger, LLC.[71]

FTIR spectroscopy on OaPAC in solution and in crystal form

Full-length OaPAC and $OaPAC_{1–137}$ proteins in solution were transferred into 10 mM of substrate in 100 mM Tris/HCl, pH 8.5, 50 mM NaCl, 5 mM $MgCl_2$ by repeated ultracentrifugation using a Vivaspin 500 filter device with a cutoff of 30 kDa (Sartorius) at 4 °C and afterwards concentrated. The concentration of the samples in crystal form was increased by sedimentation overnight and removal of the supernatant. The final concentration of the samples was 0.3–3.0 mM.

1.5 μL of the samples was placed between two BaF_2 windows, which were sealed without any drying using vacuum grease. The path length was adjusted to reach an absorbance at 1650 cm^{-1} of 0.7–1.1. Full hydration was evident from an absorbance ratio of amide I /H_2O to amide II of 2.7–3.5.

The experiments were carried out on an IFS 66/S spectrometer (Bruker) at 10 °C using a mercury cadmium telluride detector. A long wave pass filter with a cut off of 2040 cm^{-1} was used to remove stray light. The spectra were recorded at a scanner velocity of 150 kHz and a spectral resolution of 2 cm^{-1}. The Fourier Transform was performed using a zero-filling factor of 4.

The time-resolved difference spectra were obtained using the rapid-scan mode induced by a blue light LED (445 nm, 25 mW/cm^2, Philips Lumileds) with a diffusion disc placed in front. Full length OaPAC with non-hydrolysable ATP analogue ApCpp, without any substrate, crystallized OaPAC and $OaPAC_{1–137}$ were illuminated for 10 s. Full length OaPAC with ATP was illuminated for 4 s. Data were collected directly before and after the illumination with a sequence of 32, 64, 128, eight times 256 and two times 1024 scans per experiment. For full length OaPAC with ATP, with ApCpp, without any substrate, crystallized OaPAC and $OaPAC_{1–137}$ in total 16, 64, 16, 32 and 32 experiments were averaged, respectively.

For reference measurements, 4 mM of cyclic adenosine monophosphate, adenosine triphosphate, pyrophosphate and phosphate were dissolved in 100 mM Tris/HCl pH 8.5, 50 mM NaCl, 5 mM $MgCl_2$ and analyzed using an attenuated total reflection setup. 100 μL of the samples was placed on the internal reflection element with nine active reflections and the buffer was directly subtracted.

CRediT authorship contribution statement

Anaïs Chretien: Investigation, Writing – original draft, Writing – review & editing. **Marius F. Nagel:** Investigation, Writing – review & editing. **Sabine Botha:** Formal analysis, Software, Writing – review & editing. **Raphaël de Wijn:** Resources. **Lea Brings:** Resources. **Katerina Dörner:** Resources. **Huijong Han:** Resources. **Jayanath C.P. Koliyadu:** Resources. **Romain Letrun:** Resources. **Adam Round:** Resources. **Tokushi Sato:** Resources. **Christina Schmidt:** Conceptualization, Funding acquisition, Supervision. **Radu-Costin Secareanu:** Resources. **David von Stetten:** Resources. **Mohammad Vakili:** Resources. **Agnieszka Wrona:** Resources. **Richard Bean:** Resources. **Adrian Mancuso:** Resources. **Joachim Schulz:** Funding acquisition. **Arwen R. Pearson:** Conceptualization, Supervision. **Tilman Kottke:** Conceptualization, Writing – review & editing. **Kristina Lorenzen:** Conceptualization, Funding acquisition, Supervision. **Robin Schubert:** Conceptualization, Funding acquisition, Project administration, Supervision, Writing – original draft, Writing – review & editing.

DECLARATION OF COMPETING INTEREST

The authors declare that they have no known competing financial interests or personal relationships that could have appeared to influence the work reported in this paper.

Acknowledgement

S.B. was supported by the NSF Science and Technology Center award 1231306 “Biology with X-ray lasers (BioXFEL)” and the Biodesign Center for Applied Structural Discovery (CASD) at Arizona State University. A. R. P. is supported by the Federal Excellence Cluster: CUI: Advanced Imaging of Matter (EXC2056). We acknowledge the European Synchrotron Radiation Facility (ESRF) in Grenoble, France for provision of synchrotron radiation facilities to collect some of the data presented in this research. We would like to thank Dr. Gordon Leonard and Dr. Shibom Basu for assistance and support in using beamline ID23-2. Beamtimes were allocated for proposals MX-2274 and MX-2374. We acknowledge DESY (Hamburg, Germany), a member of the Helmholtz Association HGF, for the provision of experimental facilities. Parts of this research were carried out at PETRA III and we would like to thank Dr. Johanna Hakanpää for assistance in using beamline P11. Beamtime was allocated for proposal BAG-20220737. We acknowledge European XFEL in Schenefeld, Germany, for provision of X-ray free-electron laser beamtime at Scientific Instrument SPB/SFX (Single Particles, Clusters, and Biomolecules and Serial

Femtosecond Crystallography) and would like to thank the staff for their assistance.

Appendix A. Supplementary material

Supplementary material to this article can be found online at https://doi.org/10.1016/j.jmb.2024.168439.

Received 5 September 2023;
Accepted 3 January 2024;
Available online 5 January 2024

Keywords:
time-resolved crystallography;
photoreceptor;
BLUF domain;
light excitation;
signal transduction

† Current address: Center for Free-Electron Laser Science CFEL, Deutsches Elektronen-Synchrotron DESY, Hamburg, Germany.
‡ Current address: Diamond Light Source, Didcot, UK.

References

1. Hendriks, J., van der Horst, M.A., Chua, T.K., Pérez, M.Á., van Wilderen, L.J., Alexandre, M.T., et al., (2009). The Purple Phototrophic Bacteria. Photoreceptor Proteins from Purple Bacteria. Springer Science, pp. 811–837.
2. Losi, A., Gardner, K.H., Möglich, A., (2018). Blue-light receptors for optogenetic. *Chem. Rev.* **118**, 10659–10709.
3. Christie, J.M., Gawthorne, J., Young, G., Fraser, N.J., Roe, A.J., (2012). LOV to BLUF: flavoprotein contributions to the optogenetic toolkit. *Mol. Plant* **5**, 533–544.
4. Weissenberger, S., Schultheis, C., Liewald, J.F., Erbguth, K., Nagel, G., Gottschalk, A., (2011). PACα-an optogenetic tool for in vivo manipulation of cellular cAMP levels, neurotransmitter release, and behavior in Caenorhabditis elegans. *J. Neurochem.* **116**, 616–625.
5. Schröder-Lang, S., Schwärzel, M., Seifert, R., Strünker, T., Kateriya, S., Looser, J., et al., (2007). Fast manipulation of cellular cAMP level by light in vivo. *Nat. Methods* **4**, 39–42.
6. Conrad, K.S., Manahan, C.C., Crane, B.R., (2014). Photochemistry of flavoprotein light sensors. *Nat. Chem. Biol.* **10**, 801–809.
7. Efetova, M., Petereit, L., Rosiewicz, K., Overend, G., Haußig, F., Hovemann, B.T., et al., (2013). Separate roles of PKA and EPAC in renal function unraveled by the optogenetic control of cAMP levels in vivo. *J. Cell Sci.* **126**, 778–788.
8. Nagahama, T., Suzuki, T., Yoshikawa, S., Iseki, M., (2007). Functional transplant of photoactivated adenylyl cyclase (PAC) into Aplysia sensory neurons. *Neurosci. Res.* **59**, 81–88.
9. Moffat, K., (2014). Time-resolved crystallography and protein design: signalling photoreceptors and optogenetics. *Philos. Trans. R. Soc. Lond. B Biol. Sci.* **369**, 20130568.
10. Möglich, A., Ayers, R.A., Moffat, K., (2009). Design and signaling mechanism of light-regulated histidine kinases. *J. Mol. Biol.* **385**, 1433–1444.
11. Ryu, M.-H., Moskvin, O.V., Siltberg-Liberles, J., Gomelsky, M., (2010). Natural and engineered photoactivated nucleotidyl cyclases for optogenetic applications. *J. Biol. Chem.* **285**, 41501–41508.
12. Tanwar, M., Sharma, K., Moar, P., Kateriya, S., (2018). Biochemical characterization of the engineered soluble photoactivated guanylate cyclases from microbes expands optogenetic tools. *Appl. Biochem. Biotechnol.* **185**, 1014–1028.
13. Wu, Y.I., Frey, D., Lungu, O.I., Jaehrig, A., Schlichting, I., Kuhlman, B., et al., (2009). A genetically encoded photoactivatable Rac controls the motility of living cells. *Nature* **461**, 104–108.
14. Grusch, M., Schelch, K., Riedler, R., Reichhart, E., Differ, C., Berger, W., et al., (2014). Spatio-temporally precise activation of engineered receptor tyrosine kinases by light. *EMBO J.* **33**, 1713–1726.
15. Han, Y., Braatsch, S., Osterloh, L., Klug, G., (2004). A eukaryotic BLUF domain mediates light-dependent gene expression in the purple bacterium Rhodobacter sphaeroides 2.4.1. *PNAS* **101**, 12306–12311.
16. Gomelsky, M., Klug, G., (2002). BLUF: a novel FAD-binding domain involved in sensory transduction in microorganisms. *Trends Biochem. Sci.* **27**, 497–500.
17. Iseki, M., Matsunaga, S., Murakami, A., Ohno, K., Shiga, K., Yoshida, K., et al., (2002). A blue-light-activated adenylyl cyclase mediates photoavoidance in Euglena gracilis. *Nature* **415**, 1047–1051.
18. Lindner, R., Hartmann, E., Tarnawski, M., Winkler, A., Frey, D., Reinstein, J., et al., (2017). Photoactivation mechanism of a bacterial light-regulated adenylyl cyclase. *J. Mol. Biol.* **429**, 1336–1351.
19. Stierl, M., Stumpf, P., Udwari, D., Gueta, R., Hagedorn, R., Losi, A., et al., (2011). Light modulation of cellular cAMP by a small bacterial photoactivated adenylyl cyclase, bPAC, of the soil bacterium Beggiatoa. *J. Biol. Chem.* **286**, 1181–1188.
20. Ohki, M., Sugiyama, K., Kawai, F., Tanaka, H., Nihei, Y., Unzai, S., et al., (2016). Structural insight into photoactivation of an adenylate cyclase from a photosynthetic cyanobacterium. *PNAS* **113**, 6659–6664.
21. Ohki, M., Sato-Tomita, A., Matsunaga, S., Iseki, M., Tame, J.R.H., Shibayama, N., et al., (2017). Molecular mechanism of photoactivation of a light-regulated adenylate cyclase. *PNAS* **114**, 8562–8567.
22. Hirano, M., Takebe, M., Ishido, T., Ide, T., Matsunaga, S., (2019). The C-terminal region affects the activity of photoactivated adenylyl cyclase from Oscillatoria acuminata. *Sci. Rep.* **9**, 20262.
23. Gold, M.G., Gonen, T., Scott, J.D., (2013). Local cAMP signaling in disease at a glance. *J. Cell Sci.* **126**, 4537–4543.
24. Kimata, K., Takahashi, H., Inada, T., Postma, P., Aiba, H., (1997). cAMP receptor protein-cAMP plays a crucial role in glucose-lactose diauxie by activating the major glucose transporter gene in Escherichia coli. *PNAS* **94**, 12914–12919.
25. Bonetti, C., Mathes, T., van Stokkum, I.H.M., Mullen, K.M., Groot, M.-L., van Grondelle, R., et al., (2008). Hydrogen bond switching among flavin and amino acid side chains in the BLUF photoreceptor observed by ultrafast infrared spectroscopy. *Biophys. J .* **95**, 4790–4802.
26. Iwata, T., Watanabe, A., Iseki, M., Watanabe, M., Kandori, H., (2011). Strong Donation of the Hydrogen Bond of

Tyrosine during Photoactivation of the BLUF Domain. *J. Phys. Chem. Lett.* **2**, 1015–1019.
27. Stelling, A.L., Ronayne, K.L., Nappa, J., Tonge, P.J., Meech, S.R., (2007). Ultrafast structural dynamics in BLUF domains: transient infrared spectroscopy of AppA and its mutants. *J. Am. Chem. Soc.* **129**, 15556–15564.
28. Okajima, K., Fukushima, Y., Suzuki, H., Kita, A., Ochiai, Y., Katayama, M., et al., (2006). Fate determination of the flavin photoreceptions in the cyanobacterial blue light receptor TePixD (Tll0078). *J. Mol. Biol.* **363**, 10–18.
29. Richard, B., Andras, L., Allison, H., Kiri, A., Agnieszka, G., Michael, T., et al., (2013). Proteins in action: femtosecond to millisecond structural dynamics of a photoactive flavoprotein. *J. Am. Chem. Soc.* **135**, 16168–16174.
30. Barends, T.R.M., Hartmann, E., Griese, J.J., Beitlich, T., Kirienko, N.V., Ryjenkov, D.A., et al., (2009). Structure and mechanism of a bacterial light-regulated cyclic nucleotide phosphodiesterase. *Nature* **459**, 1015–1018.
31. Goings, J.J., Li, P., Zhu, Q., Hammes-Schiffer, S., (2020). Formation of an unusual glutamine tautomer in a blue light using flavin photocycle characterizes the light-adapted state. *PNAS* **117**, 26626–26632.
32. Anderson, S., Dragnea, V., Masuda, S., Ybe, J., Moffat, K., Bauer, C., (2005). Structure of a novel photoreceptor, the BLUF domain of AppA from Rhodobacter sphaeroides. *Biochemistry* **44**, 7998–8005.
33. Yuan, H., Anderson, S., Masuda, S., Dragnea, V., Moffat, K., Bauer, C., (2006). Crystal structures of the Synechocystis photoreceptor Slr1694 reveal distinct structural states related to signaling. *Biochemistry* **45**, 12687–12694.
34. Fujisawa, T., Masuda, S., (2018). Light-induced chromophore and protein responses and mechanical signal transduction of BLUF proteins. *Biophys. Rev.* **10**, 327–337.
35. Gauden, M., van Stokkum, I.H.M., Key, J.M., Lührs, D.C., van Grondelle, R., Hegemann, P., et al., (2006). Hydrogen-bond switching through a radical pair mechanism in a flavin-binding photoreceptor. *PNAS* **103**, 10895–10900.
36. Domratcheva, T., Hartmann, E., Schlichting, I., Kottke, T., (2016). Evidence for tautomerisation of glutamine in BLUF blue light receptors by vibrational spectroscopy and computational chemistry. *Sci. Rep.* **6**, 22669.
37. Hontani, Y., Mehlhorn, J., Domratcheva, T., Beck, S., Kloz, M., Hegemann, P., et al., (2023). Spectroscopic and computational observation of glutamine tautomerization in the blue light sensing using flavin domain photoreaction. *J. Am. Chem. Soc.* **145**, 1040–1052.
38. Kita, A., Okajima, K., Morimoto, Y., Ikeuchi, M., Miki, K., (2005). Structure of a cyanobacterial BLUF protein, Tll0078, containing a novel FAD-binding blue light sensor domain. *J. Mol. Biol.* **349**, 1–9.
39. Jung, A., Domratcheva, T., Tarutina, M., Wu, Q., Ko, W., Shoeman, R.L., et al., (2005). Structure of a bacterial BLUF photoreceptor: Insights into blue light-mediated signal transduction. *PNAS* **102**, 12350–12355.
40. Chitrakar, I., Iuliano, J.N., He, Y., Woroniecka, H.A., Tolentino Collado, J., Wint, J.M., et al., (2020). Structural basis for the regulation of biofilm formation and iron uptake in A. baumannii by the blue-light-using photoreceptor, BlsA. *ACS Infect. Dis.* **6**, 2592–2603.
41. Grinstead, J.S., Hsu, S.-T.-D., Laan, W., Bonvin, A.M.J.J., Hellingwerf, K.J., Boelens, R., et al., (2006). The solution structure of the AppA BLUF domain: insight into the mechanism of light-induced signaling. *Chembiochem. Eur. J. Chem. Biol.* **7**, 187–193.
42. Masuda, S., Hasegawa, K., Ono, T., (2005). Tryptophan at position 104 is involved in transforming light signal into changes of beta-sheet structure for the signaling state in the BLUF domain of AppA. *Plant Cell Physiol.* **46**, 1894–1901.
43. Masuda, S., Tomida, Y., Ohta, H., Takamiya, K.-I., (2007). The critical role of a hydrogen bond between Gln63 and Trp104 in the blue-light sensing BLUF domain that controls AppA activity. *J. Mol. Biol.* **368**, 1223–1230.
44. Karadi, K., Kapetanaki, S.M., Raics, K., Pecsi, I., Kapronczai, R., Fekete, Z., et al., (2020). Functional dynamics of a single tryptophan residue in a BLUF protein revealed by fluorescence spectroscopy. *Sci. Rep.* **10**, 2061.
45. Grigorenko, B., Polyakov, I., Nemukhin, A., (2020). Mechanisms of ATP to cAMP Conversion Catalyzed by the Mammalian Adenylyl Cyclase: A Role of Magnesium Coordination Shells and Proton Wires. *J. Phys. Chem. B* **124**, 451–460.
46. Hahn, D.K., Tusell, J.R., Sprang, S.R., Chu, X., (2015). Catalytic mechanism of mammalian adenylyl cyclase: A computational investigation. *Biochemistry* **54**, 6252–6262.
47. Lindner, R., (2018). Blue-Light-Regulated Adenylyl Cyclases, optogenetic tools and model systems for inter-domain communication. University of Heidelberg, Germany.
48. Barth, A., Mäntele, W., (1998). ATP-Induced phosphorylation of the sarcoplasmic reticulum Ca2+ ATPase: molecular interpretation of infrared difference spectra. *Biophys. J* . **75**, 538–544.
49. Stierl, M., Penzkofer, A., Kennis, J.T.M., Hegemann, P., Mathes, T., (2014). Key residues for the light regulation of the blue light-activated adenylyl cyclase from Beggiatoa sp.. *Biochemistry* **53**, 5121–5130.
50. Masuda, S., Hasegawa, K., Ono, T., (2005). Light-induced structural changes of apoprotein and chromophore in the sensor of blue light using FAD (BLUF) domain of AppA for a signaling state. *Biochemistry* **44**, 1215–1224.
51. Hasegawa, K., Masuda, S., Ono, T., (2005). Spectroscopic analysis of the dark relaxation process of a photocycle in a sensor of blue light using FAD (BLUF) protein Slr1694 of the cyanobacterium Synechocystis sp. PCC6803. *Plant Cell Physiol.* **46**, 136–146.
52. Schroeder, C., Werner, K., Otten, H., Krätzig, S., Schwalbe, H., Essen, L.-O., (2008). Influence of a joining helix on the BLUF domain of the YcgF photoreceptor from Escherichia coli. *Chembiochem. Eur. J. Chem. Biol.* **9**, 2463–2473.
53. Dragnea, V., Arunkumar, A.I., Lee, C.W., Giedroc, D.P., Bauer, C.E., (2010). A Q63E Rhodobacter sphaeroides AppA BLUF domain mutant is locked in a pseudo-light-excited signaling state. *Biochemistry* **49**, 10682–10690.
54. Domratcheva, T., Grigorenko, B.L., Schlichting, I., Nemukhin, A.V., (2008). Molecular models predict light-induced glutamine tautomerization in BLUF photoreceptors. *Biophys. J* . **94**, 3872–3879.
55. Yuan, H., Dragnea, V., Wu, Q., Gardner, K.H., Bauer, C.E., (2011). Mutational and structural studies of the PixD BLUF output signal that affects light-regulated interactions with PixE. *Biochemistry* **50**, 6365–6375.
56. Hasegawa, K., Masuda, S., Ono, T., (2006). Light induced structural changes of a full-length protein and its BLUF

domain in YcgF(Blrp), a blue-light sensing protein that uses FAD (BLUF). *Biochemistry* **45**, 3785–3793.
57. Barth, A., Zscherp, C., (2002). What vibrations tell us about proteins. *Q. Rev. Biophys.* **35**, 369–430.
58. Collado, J.T., Iuliano, J.N., Pirisi, K., Jewlikar, S., Adamczyk, K., Greetham, G.M., et al., (2022). Unraveling the photoactivation mechanism of a light-activated adenylyl cyclase using ultrafast spectroscopy coupled with unnatural amino acid mutagenesis. *ACS Chem. Biol.* **17**, 2643–2654.
59. Sadeghian, K., Bocola, M., Schütz, M., (2008). A conclusive mechanism of the photoinduced reaction cascade in blue light using flavin photoreceptors. *J. Am. Chem. Soc.* **130**, 12501–12513.
60. Jung, A., Reinstein, J., Domratcheva, T., Shoeman, R.L., Schlichting, I., (2006). Crystal structures of the AppA BLUF domain photoreceptor provide insights into blue light-mediated signal transduction. *J. Mol. Biol.* **362**, 717–732.
61. Wu, Q., Gardner, K.H., (2009). Structure and insight into blue light-induced changes in the BlrP1 BLUF domain. *Biochemistry* **48**, 2620–2629.
62. Tokonami, S., Onose, M., Nakasone, Y., Terazima, M., (2022). Slow conformational changes of blue light sensor BLUF proteins in milliseconds. *J. Am. Chem. Soc.* **144**, 4080–4090.
63. Han, H., Round, E., Schubert, R., Gül, Y., Makroczyová, J., Meza, D., et al., (2021). The XBI BioLab for life science experiments at the European XFEL. *J. Appl. Cryst.* **54**, 7–21.
64. Flot, D., Mairs, T., Giraud, T., Guijarro, M., Lesourd, M., Rey, V., et al., (2010). The ID23-2 structural biology microfocus beamline at the ESRF. *J. Synchrotron Radiat.* **17**, 107–118.
65. Burkhardt, A., Pakendorf, T., Reime, B., Meyer, J., Fischer, P., Stübe, N., et al., (2016). Status of the crystallography beamlines at PETRA III. *Eur. Phys. J. Plus* **131**, 56.
66. Kabsch, W., (2010). XDS. *Acta Crystallogr. Sect. D, Biol. Crystallogr.* **66**, 125–132.
67. Evans, P.R., Murshudov, G.N., (2013). How good are my data and what is the resolution? *Acta Crystallogr. Sect. D, Biol. Crystallogr.* **69**, 1204–1214.
68. Agirre, J., Atanasova, M., Bagdonas, H., Ballard, C.B., Baslé, A., Beilsten-Edmands, J., et al., (2023). The CCP4 suite: integrative software for macromolecular crystallography. *Acta Crystallogr. Sect. D, Struct. Crystallogr.* **79**, 449–461.
69. Adams, P.D., Afonine, P.V., Bunkóczi, G., Chen, V.B., Davis, I.W., Echols, N., et al., (2010). PHENIX: a comprehensive Python-based system for macromolecular structure solution. *Acta Crystallogr. Sect. D, Biol. Crystallogr.* **66**, 213–221.
70. Emsley, P., Lohkamp, B., Scott, W.G., Cowtan, K., (2010). Features and development of Coot. *Acta Crystallogr. Sect. D, Biol. Crystallogr.* **66**, 486–501.
71. Schrödinger, L., DeLano, W., 2020. PyMOL.
72. Vakili, M., Bielecki, J., Knoška, J., Otte, F., Han, H., Kloos, M., et al., (2022). 3D printed devices and infrastructure for liquid sample delivery at the European XFEL. *J. Synchrotron Radiat.* **29**, 331–346.
73. Mancuso, A.P., Aquila, A., Batchelor, L., Bean, R.J., Bielecki, J., Borchers, G., et al., (2019). The single particles, clusters and biomolecules and serial femtosecond crystallography instrument of the European XFEL: Initial installation. *J. Synchrotron Radiat.* **26**, 660–676.
74. Pergament, M., Palmer, G., Kellert, M., Kruse, K., Wang, J., Wissmann, L., et al., (2016). Versatile optical laser system for experiments at the European X-ray free-electron laser facility. *Opt. Express* **24**, 29349–29359.
75. Palmer, G., Kellert, M., Wang, J., Emons, M., Wegner, U., Kane, D., et al., (2019). Pump-probe laser system at the FXE and SPB/SFX instruments of the European X-ray Free-Electron Laser Facility. *J. Synchrotron Radiat.* **26**, 328–332.
76. Koliyadu, J.C.P., Letrun, R., Kirkwood, H.J., Liu, J., Jiang, M., Emons, M., et al., (2022). Pump-probe capabilities at the SPB/SFX instrument of the European XFEL. *J. Synchrotron Radiat.* **29**, 1273–1283.
77. Grünbein, M.L., Stricker, M., Nass Kovacs, G., Kloos, M., Doak, R.B., Shoeman, R.L., et al., (2020). Illumination guidelines for ultrafast pump-probe experiments by serial femtosecond crystallography. *Nat. Methods* **17**, 681–684.
78. Allahgholi, A., Becker, J., Delfs, A., Dinapoli, R., Goettlicher, P., Greiffenberg, D., et al., (2019). The adaptive gain integrating pixel detector at the European XFEL. *J. Synchrotron Radiat.* **26**, 74–82.
79. Fangohr, H., Aplin, S., Barty, A., Beg, M., Bondar, V., Boukhelef, D., et al. (Eds.), 2018. Data Analysis Support in Karabo at European XFEL.
80. Mariani, V., Morgan, A., Yoon, C.H., Lane, T.J., White, T. A., O'Grady, C., et al., (2016). OnDA: online data analysis and feedback for serial X-ray imaging. *J. Appl. Cryst.* **49**, 1073–1080.
81. White, T.A., Kirian, R.A., Martin, A.V., Aquila, A., Nass, K., Barty, A., et al., (2012). CrystFEL : a software suite for snapshot serial crystallography. *J. Appl. Cryst.* **45**, 335–341.
82. Turkot, O., Dall'Antonia, F., Bean, R.J., E, J., Fangohr, H., Ferreira de Lima, D.E., et al. Towards automated analysis of serial crystallography data at European XFEL, p. 45.
83. Barty, A., Kirian, R.A., Maia, F.R.N.C., Hantke, M., Yoon, C.H., White, T.A., et al., (2014). Cheetah: software for high-throughput reduction and analysis of serial femtosecond X-ray diffraction data. *J. Appl. Cryst.* **47**, 1118–1131.
84. Powell, H.R., Johnson, O., Leslie, A.G.W., (2013). Autoindexing diffraction images with iMosflm. *Acta Crystallogr. Sect. D, Biol. Crystallogr.* **69**, 1195–1203.
85. Gevorkov, Y., Yefanov, O., Barty, A., White, T.A., Mariani, V., Brehm, W., et al., (2019). XGANDALF - extended gradient descent algorithm for lattice finding. *Acta Crystallogr. Sect. A, Found. Adv.* **75**, 694–704.
86. Duisenberg, A.J.M., (1992). Indexing in single-crystal diffractometry with an obstinate list of reflections. *J. Appl. Cryst.* **25**, 92–96.
87. White, T.A., (2019). Processing serial crystallography data with CrystFEL: a step-by-step guide. *Acta Crystallogr. D Struct. Biol.* **75**, 219–233.
88. de Zitter, E., Coquelle, N., Oeser, P., Barends, T.R.M., Colletier, J.-P., (2022). Xtrapol8 enables automatic elucidation of low-occupancy intermediate-states in crystallographic studies. *Commun. Biol.* **5**, 640.